Numerical Prediction of Flame Images in the Visible Spectrum Range*

José C.F. PEREIRA**, Pedro J. COELHO**,
Jorge M.P. ROCHA** and Maria G. CARVALHO**

In this paper a numerical technique is presented to predict the image of a free flame in the visible spectrum range from the computational results obtained with a fluid flow and combustion code. The numerical technique is composed of two submodels. The first one is a mathematical model based on the solution of the time-averaged form of the conservation equations for mass, momentum and energy. The output results are used as input data for the second submodel which is able to predict the flame image/brightness. This submodel is based on the integration of the radiative heat transfer equation along selected directions. The basic assumption of this submodel is that radiation is mainly due to soot in the visible range of the spectrum. The model was applied to a turbulent propane free flame for which experimental temperature measurements and digitized flame images were available. The predicted temperatures are in reasonable agreement with the experimental data, and the shape of the predicted flame image is qualitatively similar to that of the digitized flame image. Overall, the model proved to be a useful engineering predictive tool for numerical visualization of sooty flames.

Key Words: Mathematical Modeling; Flame Image Prediction; Flame Brightness; Radiative Heat Transfer; Sooty Flame

1. Introduction

The optimum operation of a furnace depends upon the flame characteristics which influence the efficiency, pollutant emission and overall safety of the installations. Therefore, flame visualization is very important in the control of industrial furnaces and power plants. Many furnaces have already installed normal CCD cameras that detect the flame in the visible spectrum range. From the digitized flame image, several relevant features related with the performance of the burning process can be extracted. These features can be used by a flame classifier designed and optimized according to previously acquired standard patterns[1]. Each flame class corresponds to a specific operating point of the furnace. Therefore, this information can be used for monitoring and diagnosis and fed back to the control and supervisor systems.

Although radiation transfer in the visible range has been studied for many decades, we are not aware of any studies related to the attempt to predict a turbulent flame image. Nevertheless, the above discussion has shown that a predictive method of the digitized flame image may serve as a powerful tool in design and on-line operation control strategies of practical combustion systems. Thus, the main objective of the present work is to outline an engineering predictive tool to simulate a CCD camera image.

The numerical technique developed is composed of two submodels. The first one is a mathematical model for the prediction of the flame properties based on the solution of the time-averaged form of the conservation equations for mass, momentum and energy. This model must provide the information required by the second submodel (absorption coefficient and temperature distribution) and its details are not important for our objective: the prediction of flame images. Any other model allowing the calculation of those properties can be used. The second submodel, which is able to predict the flame image/brightness, relies on the assumption that radiation in the visible range of the spectrum is mainly due

* Received 23rd February, 1993.
** Instituto Superior Técnico, Technical University of Lisbon, Mechanical Engineering Department, Av. Rovisco Paris, 1096 Lisboa Codex, Portugal

to soot. It is based on the integration of the radiative heat transfer equation along selected directions.

The next section describes the mathematical and numerical models used to predict the flow field, the chemical species and temperature distributions, and the absorption coefficient of the medium. This is followed in the third section by a description of the numerical procedure used to predict the flame image. The results obtained for a vertical turbulent propane free flame are described in the fourth section and the paper ends with a summary of the study.

2. Prediction of Flame Properties

To predict the flame image, it is necessary to know the temperature field and the absorption coefficient of the medium. The procedure used to calculate these quantities is irrelevant as far as the flame image prediction is concerned. An outline of the mathematical model used in the present study to predict the flame properties is given below. However, other fluid flow and combustion codes may also be used.

2.1 Mean flow conservation equations

The incompressible, time-averaged forms of the conservation equations for mass, momentum and scalar quantities for a steady turbulent high Reynolds number flow with chemical reaction can be written, in Cartesian coordinates, as follows:

Continuity

$$\frac{\partial \rho U_i}{\partial x_i}=0, \tag{1}$$

Momentum

$$\frac{\partial}{\partial x_j}(\rho U_j U_i)=-\frac{\partial p}{\partial x_i}-\frac{\partial}{\partial x_j}(\rho\langle u_i u_j\rangle), \tag{2}$$

Scalar

$$\frac{\partial}{\partial x_j}(\rho U_j \Theta)=-\frac{\partial}{\partial x_j}(\rho\langle u_i\theta\rangle)+S_\Theta, \tag{3}$$

where U_j and u_j are the mean and fluctuating velocity components along direction x_j, respectively, p is the pressure, ρ is the density, Θ and θ stand for the mean and fluctuating values of scalar properties such as temperature, enthalpy and mixture fraction, S_θ represents a source/sink of the scalar quantity and the angle brackets denote a mean value.

2.2 Turbulence model

The mean flow equations are closed by the k-ε eddy viscosity/diffusivity model which comprises transport equations for the turbulent kinetic energy, k, its dissipation rate, ε, and constitutive relations for the Reynolds stresses $\langle u_i u_j\rangle$ and turbulent scalar fluxes $\langle u_i\theta\rangle$:

$$-\rho\langle u_i u_j\rangle=\mu_t\left(\frac{\partial U_i}{\partial x_j}+\frac{\partial U_j}{\partial x_i}\right)-\rho\frac{2}{3}\delta_{ij}k \tag{4}$$

and

$$-\rho\langle u_j\theta\rangle=\rho\frac{\mu_t}{\sigma_\theta}\frac{\partial \Theta}{\partial x_j}, \tag{5}$$

$$\frac{\partial}{\partial x_j}(\rho U_j k)=\frac{\partial}{\partial x_j}\left[\frac{\mu_t}{\sigma_k}\frac{\partial k}{\partial x_j}\right]+P-\rho\varepsilon \tag{6}$$

$$\frac{\partial}{\partial x_j}(\rho U_j \varepsilon)=\frac{\partial}{\partial x_j}\left[\frac{\mu_t}{\sigma_\varepsilon}\frac{\partial \varepsilon}{\partial x_j}\right]+C_{\varepsilon 1}\frac{P}{\tau_m}-C_{\varepsilon 2}\rho\frac{\varepsilon}{\tau_m} \tag{7}$$

$$P\equiv-\rho\langle u_i u_j\rangle\frac{\partial U_i}{\partial x_j}. \tag{8}$$

In these equations P is the production of turbulent kinetic energy and δ_{ij} is the Kronecker tensor. The eddy viscosity μ_t and the characteristic time scale of the turbulent mechanical field τ_m are given by $\mu_t=\rho C_\mu\frac{k^2}{\varepsilon}$ and $\tau_m=\frac{k}{\varepsilon}$, respectively. Standard values were assigned to all the constants of the model[2]: C_μ, $C_{\varepsilon 1}$, $C_{\varepsilon 2}$, σ_k, σ_ε, and σ_θ.

The calculation of fluctuations of a scalar quantity requires the solution of a transport equation for the variance $\langle\theta^2\rangle$:

$$\frac{\partial \rho U_j\langle\theta^2\rangle}{\partial x_j}=\frac{\partial}{\partial x_j}\left[\frac{\mu_t}{\sigma_\theta}\frac{\partial\langle\theta^2\rangle}{\partial x_j}\right]+2P_\theta-2\rho\varepsilon_\theta, \tag{9}$$

where P_θ and ε_θ are the production and dissipation rates of scalar θ, respectively. In the majority of the previous studies, the dissipation rate of the scalar variance ε_θ has been calculated assuming that the ratio of the characteristic time scale of turbulent mechanical and scalar fields is constant. Hence, ε_θ is given by:

$$2\varepsilon_\theta=\frac{1}{R}\frac{\varepsilon}{k}\langle\theta^2\rangle, \tag{10}$$

and a constant value is prescribed for R. However, it has been shown experimentally[3] that under buoyancy effects (or chemical reaction), the value of R is not constant and it can be rather different from 0.5 (a value generally accepted for passive scalar dispersion). Hence, a more general and physically meaningful route to calculate ε_θ is to solve a transport equation for this quantity (see, e.g., Ref. 4):

$$\frac{\partial \rho U_j\varepsilon_\theta}{\partial x_j}=\frac{\partial}{\partial x_j}\left[\frac{\mu_t}{\sigma_{\varepsilon\theta}}\frac{\partial \varepsilon_\theta}{\partial x_j}\right]+C_{P1}\frac{\varepsilon_\theta}{\langle\theta^2\rangle}P_\theta+C_{P2}\frac{\varepsilon_\theta}{k}P-C_{D1}\rho\frac{\varepsilon_\theta^2}{\langle\theta^2\rangle}-C_{D2}\rho\frac{\varepsilon_\theta}{\tau_m}. \tag{11}$$

In related studies, the following values were assigned to the constants: $C_{P1}=1.8$ (see Ref. 5), $C_{P2}=0.72$ (see Ref. 6), $C_{D1}=2.03$ and $C_{D2}=0.88$ (see Ref. 7). In the present study, the values of the constants C_{P1} and C_{P2} were increased by 15% since the new constants yield better agreement with the experimental data.

2.3 Combustion model

The instantaneous scalar field was obtained using the laminar flamelet model[8] for propane-air diffusion flames. The stochastic behavior of the turbulence is

introduced by means of a pdf of the mixture fraction, which is supposed to obey a clipped normal distribution[9]. The mean values of density, temperature and concentration of the species C_3H_8, O_2, N_2, CO_2, CO, OH, O, H_2O, H_2 and H were obtained by integration of the relationships between those variables and the mixture fraction weighted by the pdf, over the mixture fraction range. When flame radiation is accounted for, the relationship between instantaneous values of enthalpy and mixture fraction is no longer linear. In this study, a piecewise linear relationship was assumed[10].

2.4 Soot formation and oxidation models

The distinctive feature of a propane flame is its significant soot content which influences the optical behavior of the flame. Soot concentration was predicted by solving the scalar transport equation (3) with the source term calculated as the difference between the soot formation rate S_f and the soot consumption rate S_d. A simple global expression[11] was chosen to characterize soot production:

$$S_f = C_f p_{fu} \phi^n \exp\left(-\frac{E}{RT_g}\right), \tag{12}$$

where p_{fu} is the partial pressure of the fuel, ϕ is the equivalence ratio, E is the activation energy, R is the gas constant and T_g is the gas temperature. The following values were assigned to the constants of the model: $C_f = 0.01\ \mathrm{kgN^{-1}m^{-1}s^{-1}}$, and $n=3$. Soot production is essentially zero for equivalence ratios, ϕ, lower than the incipient sooting limit and higher than a value corresponding roughly to the upper flammability limit. These lower and upper limits were set to be 2 and 8, respectively.

A simple method to estimate the soot burning rate has been proposed by Magnussen and Hjertager[12] who, following conventional turbulence concepts, presume that the mixing rate is proportional to the soot concentration and to the reciprocal of the time scale of the turbulent mechanical field τ_m. Their expression for the soot consumption rate is:

$$S_d = A m_s (\varepsilon/k) \tag{13}$$

where A is a constant of the model and m_s is the soot mass fraction. This relation is not satisfactory in regions where the reaction rate is limited by oxygen deficiency. In this case Magnussen and Hjertager propose:

$$S_d = A\left(\frac{m_{ox}}{m_s s_s + m_{fu} s_{fu}}\right) m_s \left(\frac{\varepsilon}{k}\right) \tag{14}$$

where s_s and s_{fu} are the soot and fuel stoichiometric ratios, and m_{ox} and m_{fu} are the oxygen and fuel mass fractions, respectively. The alternative which yields the smallest consumption rate is used.

2.5 Radiation Model

The discrete transfer method[13], which combines the virtues of the zonal, Monte Carlo and flux methods, was applied in the present study. The emissivity of the medium was calculated using the mixed grey and clear gas formulation[14] extended to account for soot. The constants and weighting coefficients determined by Truelove[15] were employed.

2.6 Numerical Model

The governing equations are solved using a finite-volume/finite difference method and employing a staggered grid variable arrangement. The equations are integrated over each control volume in the computational domain and the Gauss divergence theorem is applied. In the discretization procedure, the fluxes through the boundaries of each control volume must be related with the nodal values. The diffusive terms are discretized using central differences and the convective terms are discretized using the hybrid upwind/central difference scheme.

An elliptic solver especially adapted for free flows and in particular for free jets was used in the computations[16]. Boundary conditions are prescribed along all boundaries. At a distance far enough from the jet centerline, atmospheric pressure is prescribed and entrainment velocities are implicitly calculated using the radial momentum equation. The SIMPLE algorithm was chosen for the pressure-correction scheme and the strongly implicit procedure was employed for the solution of the algebraic sets of discretized equations.

3. Prediction of Flame Image

The flame properties predicted by the model described above are used as input data for the technique developed for the prediction of the flame image.

The basic assumptions of the numerical model for the prediction of the flame image/brightness are the following.

(i) The CCD camera only detects radiation in the visible range of the spectrum. This assumption is a good one provided that the CCD camera has an appropriate filter.

(ii) For the propane flame considered here, radiation in the visible range is mainly due to soot. This is a good assumption since the main absorption bands of the combustion gas products are all located in the infrared range of the spectrum. The contribution from CH, OH and C_2 has been neglected as well as transitions of electrons between energy levels.

(iii) Once the temperature and species concentration fields are known, the mean absorption coefficient can be related with the spectral one via the Planck's mean absorption coefficient. This assumption is valid for an optically thin medium. Therefore, the control volumes should be small enough to ensure that this

assumption is valid.

The radiative transfer equation (RTE) in a Lagrangian coordinate system can be written as:

$$\frac{1}{c}\frac{dI_\nu}{dt}=-(\varkappa_\nu+\sigma_\nu)I_\nu+\eta_\nu+\frac{\sigma_\nu}{4\pi}\times\int_{\Delta\nu'}\int_{\Omega'=4\pi}\Phi_\nu(\vec{s}'\rightarrow\vec{s}\,;\ \nu'\rightarrow\nu)I_{\nu'}(\vec{s}')d\Omega'd\nu' \tag{15}$$

where I_ν is the spectral radiation intensity, $\varkappa_\nu$, σ_ν and η_ν are the spectral absorption, scattering and emission coefficients, respectively, and c is the velocity of light in the medium. The phase function $\Phi_\nu(\vec{s}'\rightarrow\vec{s}\,;\ \nu'\rightarrow\nu)d\Omega'd\nu'/4\pi$ represents the probability that radiation of frequency ν' propagating in the direction $\vec{s}'$ and confined within the solid angle $d\Omega'$ is scattered through the angle $(\vec{s}',\ \vec{s})$ into the solid angle $d\Omega$ and the frequency interval $d\nu$. Assuming that Kirchhoff's law is valid, the emission coefficient η_ν can be expressed as:

$$\eta_\nu=\varkappa_\nu n_\nu^2 I_{b\nu}, \tag{16}$$

where n_ν is the real part of the complex spectral index of refraction. The RTE is a mathematical statement of the conservation of energy principle for a monochromatic pencil of radiation in the direction $\vec{s}$. It is an integrodifferential equation that is very difficult to solve exactly for a multidimensional geometry. Therefore, some simplifications are necessary to solve it.

In gaseous flames, the scattering coefficient of the medium is negligible and the RTE becomes a linear differential equation which is much easier to solve. If, in addition, the spectral refraction index is equal to one and the coordinate s lies in the $\vec{s}$ direction, the quasi-steady state RTE is given by:

$$\frac{dI_\nu}{ds}=-\varkappa_\nu(I_\nu-I_{b\nu}). \tag{17}$$

This equation may be integrated analytically, yielding:

$$I_{\nu n+1}=I_{\nu n}e^{-\varkappa_\nu l}+I_{b\nu}(1-e^{-\varkappa_\nu l}) \tag{18}$$

where $I_{\nu n}$ and $I_{\nu n+1}$ are, respectively, the values of intensity entering and leaving any control volume n that the ray has crossed and l is the distance travelled by the ray within the control volume. In order to apply this equation, knowledge of the absorption coefficient is required.

The problem of computing the absorption coefficient of soot clouds can be attacked from a fundamental point of view by means of the well-known Lorenz-Mie theory which solves the problem of scattering of a plane wave by a spherical, homogeneous, isotropic particle of arbitrary diameter by giving the solution of Maxwell's field equation with appropriate boundary conditions[17),(18)]. To interpret soot data, the complete Lorenz-Mie theory is rarely used because of its reputed difficulty and also because it could be argued that soot particles are not spherical, homogeneous or isotropic[19]. In multidimensional radiative transfer analysis, use of Mie codes is impractical. Therefore, it is desirable to have simple approximations. An extensively used soot absorption coefficient is[20]:

$$\varkappa_\lambda=Af_v/\lambda \tag{19}$$

where f_v is the volume fraction of soot particles and A is a coefficient dependent on the type of fuel. Hottel and Sarofim[14] have suggested the value of 7 for typical soot particles observed in combustion chambers. Siegel[21] has analyzed the available experimental data for several flames yielding different values of A for different types of fuels. Based on that study, the present work uses $A=4.9$, a typical value for propane flames.

The absorption coefficient can be related with the spectral absorption coefficient by the following definition

$$\bar{\varkappa}_{\lambda1,\,\lambda2}=\frac{\int_{\lambda1}^{\lambda2}E_{b\lambda}\varkappa_\lambda d\lambda}{\int_{\lambda1}^{\lambda2}E_{b\lambda}d\lambda} \tag{20}$$

where $\lambda1$ and $\lambda2$ represent the limits of the spectrum of electromagnetic radiation and the black body emissive power, $E_{b\lambda}$, is given by Planck's law.

The numerical procedure proposed in this work to predict the flame image/brightness is based on the integration of the RTE along selected directions. This procedure may be summarized as follows (see Figs. 1 and 2):

(i) Transform the predicted 2D-axisymmetric temperature and soot concentration fields into a 3D cylindrical space.

(ii) Locate the virtual CCD camera at a point $(x_c,\ y_c,\ z_c)$ in the 3D space.

(iii) Define a screen limited by the boundaries of the 3D physical domain as viewed from the CCD camera. This screen is divided into a number of $(m\times n)$ cells or "pixels".

(iv) For each one of the $(m\times n)$ cells on the screen:

(a) Select the direction defined by the position of the CCD camera $(x_c,\ y_c,\ z_c)$ and the center of the cell $(y_s,\ z_s)$.

(b) Trace a ray along the selected direction from point $(x_o,\ y_o,\ z_o)$ at the outer boundary of the flame towards the position of the CCD camera.

(c) Integrate the RTE for a solid angle defined by the selected direction from $(x_o,\ y_o,\ z_o)$ to $(x_1,\ y_1,\ z_1)$. It is useless to continue the integration up to $(x_c,\ y_c,\ z_c)$ since the absorption coefficient is negligible between $(x_1,\ y_1,\ z_1)$ and $(x_c,\ y_c,\ z_c)$. This integration yields the radiation intensity received by cell $(y_s,\ z_s)$.

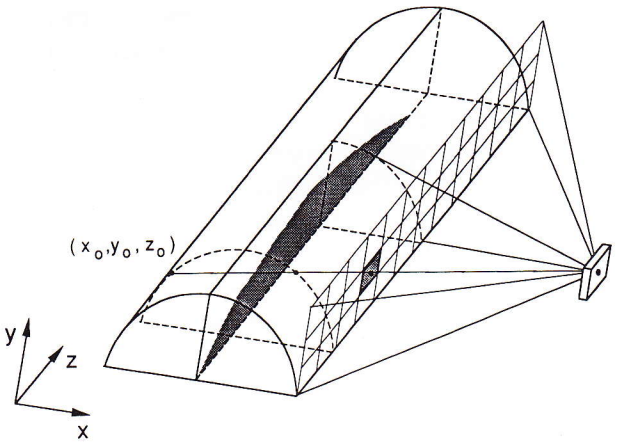

Fig. 1 Flow geometry and reference space

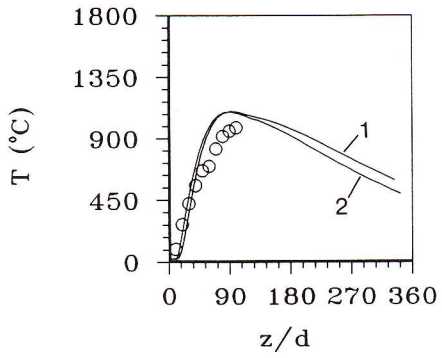

Fig. 3 Predicted (solid line) and experimental (symbols) temperature profiles along the centerline (1—32×24 grid nodes; 2—64×46 grid nodes)

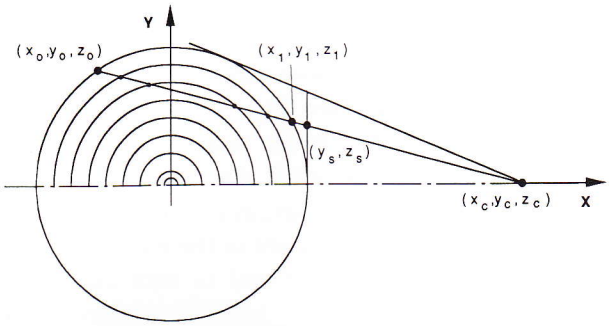

Fig. 2 Integration path

Fig. 4 Predicted (solid line) and experimental (symbols) radial temperature profiles (1—32×24 grid nodes; 2—64×46 grid nodes)

(v) Normalize the radiation intensity at each cell by the maximum value obtained. This procedure yields the predicted flame image/brightness.

4. Results and Discussion

The model was applied to the prediction of a turbulent, vertical, free jet propane flame. The flame was formed on a round nozzle with an exit diameter of $d=5$ mm. The Reynolds and the Froude numbers based on the exit diameter are 2.04×10^4 and 6.9×10^3, respectively. Temperature measurements were carried out by Fernandes et al.[22] using butt-welded thermocouples of 0.040-mm-diameter Pt/Pt-13% Rh wires. The scatter in the measured temperature profiles suggests a maximum uncertainty of 30K. Further details about the measurements may be found in Ref. 22.

Calculations were performed using two grids with 32×24 and 62×46 control volumes. The difference between the numerical solutions is very small as shown in Figs. 3 and 4. Hence, the numerical solution may be considered grid-independent.

Figure 3 shows the mean temperature profile along the centerline. The temperature increases along the centerline up to $z/d\cong90-100$ due to the heat transferred from the reaction zone where combustion takes place. Comparison with the measurements reveals a delay at the beginning of the temperature rise. This means that the transport of fuel from the central cool region to the surrounding circular mixing layer is not correctly described. The observed discrepancy may be due to the inability of the model to represent the large-scale engulfment of air and intermittence phenomena. The predited temperature increases at a higher rate than the experimental data and there is a slight overprediction between $z/d=60$ and $z/d=100$. There are no measurements available further downstream, and the calculated temperatures decrease slowly due to heat released to the surroundings.

Radial profiles of the mean temperature across several axial stations are displayed in Fig. 4. Globally, an acceptable agreement is observed between the measurements and the predictions. The predicted peak temperatures at the first few stations are in good agreement with the data. Notice that this agreement was only obtained when the transport equation for the dissipation rate of mixture fraction variance was solved. The thickness of the reaction zone near the burner is overpredicted and this may be due to an overestimation of the thermal diffusivity. As we move downstream, the peak temperature in the radial profiles decreases and moves away from the centerline, up to $z/d\cong60$. Further downstream, the peak temperature tends to disappear due to thermal diffusion and at $z/d=100$, the maximum temperature is already found at the centerline. All these features are correctly predicted by the model.

Figure 5 shows the predicted contours of several flame properties. The temperature contours display the features highlighted above. There is a radial double-peak distribution in the reaction zone up to $z/d\cong90$, where the combustion process is dominated by fuel pyrolysis, soot formation and gas-phase oxidation. Further downstream, the temperature decreases axially and radially with the maximum temperature occurring at the centerline. The fuel mass fraction contours show that the maximum values occur at the centerline. As combustion takes place, the fuel mass fraction decreases in both directions (axial and radial).

The distributions of soot concentration and mean absorption coefficient (see Figs. 5(c) and 5(d)) in the visible range are closely related. In fact, the spectral absorption coefficient due to soot is proportional to the volumetric fraction of soot. Therefore, the mean absorption coefficient in the visible range is also approximately proportional to soot concentration. Soot is formed in the fuel-rich region of the flame and maximum concentration is found at the centerline and areas adjacent to it, between $z/d=70$ and $z/d=140$. So, the higher absorption coefficients are predicted also in this region.

Flame brightness is calculated according to the methodology outlined in the previous section using the temperature and absorption coefficient distributions presented in Figs. 5(a) and 5(d) as input data. The flame brightness is strongly dependent on the absorption coefficient of the medium, as well as on the fourth power of temperature. However, higher temperatures occur near the burner in a region where the amount of soot formed is still limited. Therefore, the absorption coefficient is too small and the radiation intensity is only marginally affected. Further downstream, between $z/d=70$ and $z/d=140$, although the maximum temperatures decrease, soot concentration is quite high, yielding high absorption coefficients. Since the temperature remains relatively high, the radiation intensity is strongly affected and the flame brightness is at a maximum. At stations where $z/d>140$, soot concentration decreases due to oxidation and diffusion. Therefore, the absorption coefficient decreases as well as the temperature. Hence, the flame brightness is strongly dependent on the absorption coefficient distribution.

Three-dimensional views of the flame brightness are presented in Fig. 6. It can be seen that the shapes of the predicted image and the digitized flame image

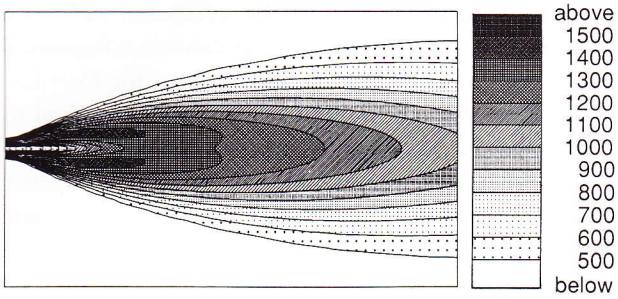

a) Temperature (K)

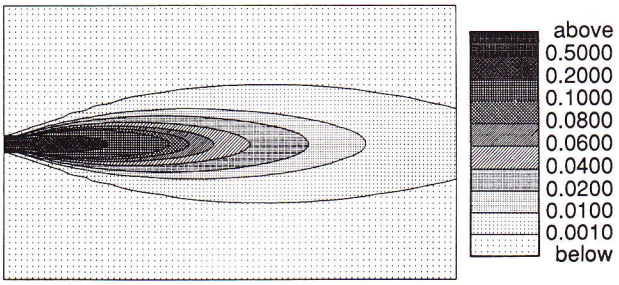

b) Fuel mass fraction

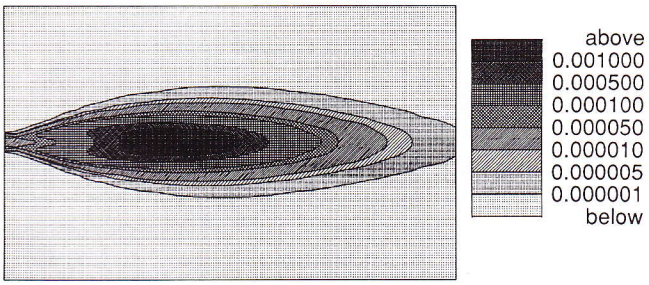

c) Soot concentration (kgm^{-3})

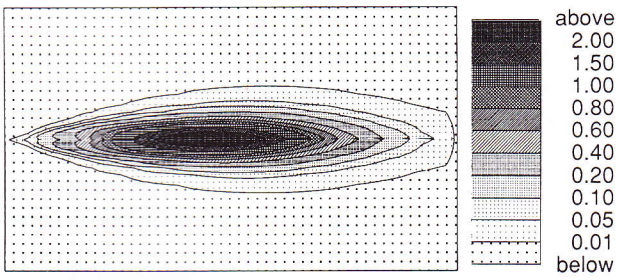

d) Mean absorption coefficient in the visible range

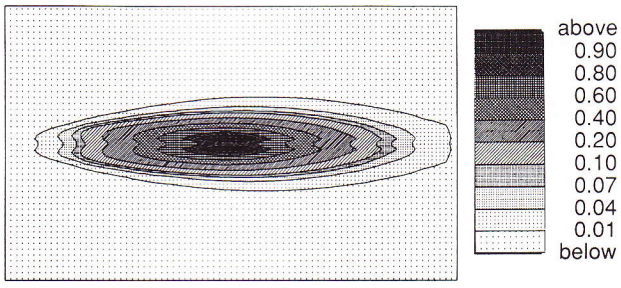

e) Flame brightness

Fig. 5 Predicted contours of flame properties

obtained with a CCD camera reveal similar trends, although the experimental image is not smooth. The predicted shape is almost symmetric if cut by a plane crosswise through the point of maximum brightness. The experimental image has a rounder contour between the burner and the point of maximum brightness and a steeper contour at downstream locations. The discrepancies between the two images may be mainly attributed to the shortcomings of the soot formation model used. Uncertainties in soot concentration lead to uncertainties in the absorption

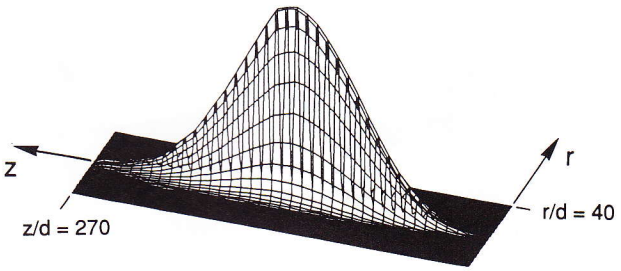

a) Predictions ($Re=2.04\times10^3$)

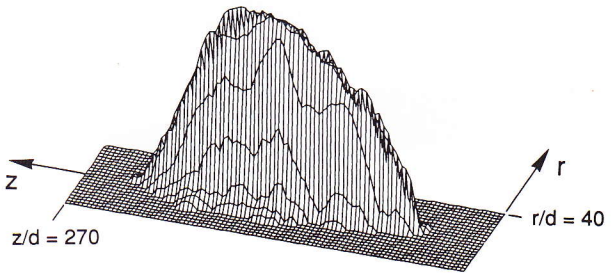

b) Measurements ($Re=2.04\times10^3$)

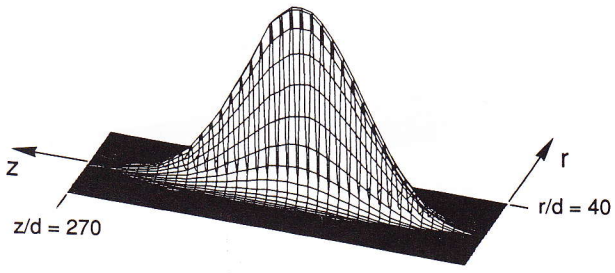

c) Predictions ($Re=1.57\times10^3$)

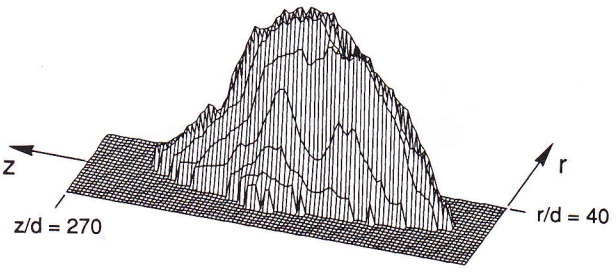

d) Measurements ($Re=1.57\times10^3$)

Fig. 6 Perspective of the flame brightness

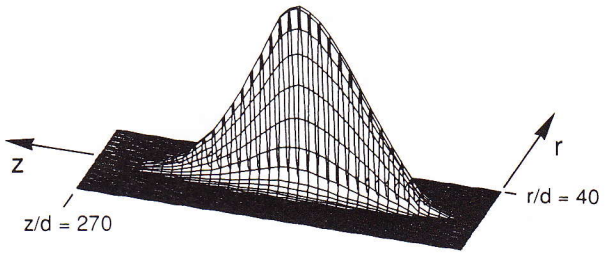

a) $x=3$ m, $z/d=0$

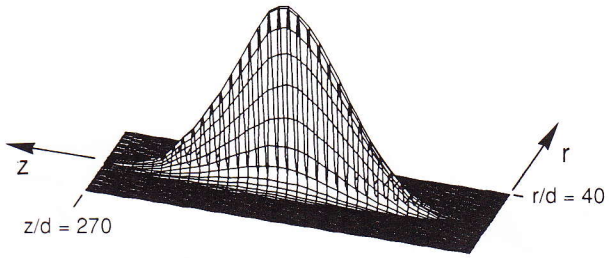

b) $x=3$ m, $z/d=270$

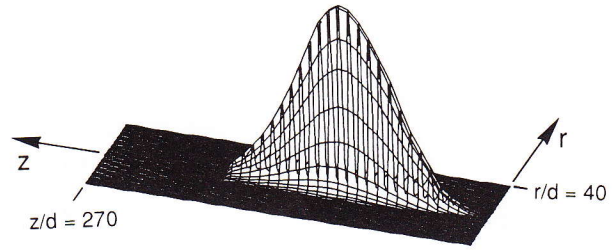

c) $x=1$ m, $z/d=0$

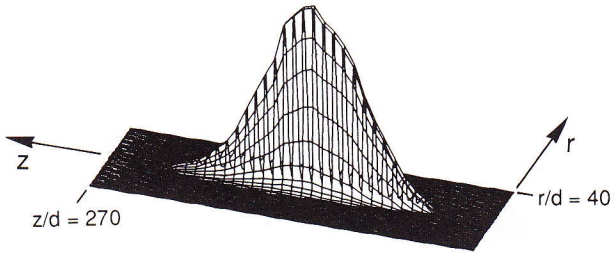

d) $x=1$ m, $z/d=135$

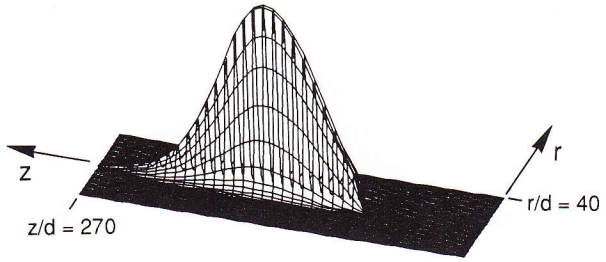

e) $x=1$ m, $z/d=270$

Fig. 7 Influence of the position of the CCD camera on the predicted flame brightness

coeffiient and ultimately in the computed radiation intensity obtained with the CCD camera. Figures 6 (c) and 6 (d) show similar perspectives for $Re=1.57\times10^3$. The shape of the images is almost identical to the previous ones. There is only a slight axial displacement of the images. At higher Reynolds number the maximum brightness occurs further downstream.

The calculation of the flame brightness just presented assumed that the CCD camera was located at a distance of 3 m from the centerline ($x=3$ m in Fig. 1) and at the axial station $z/d=135$. Several 3D views of the predicted flame image brightness are displayed in Fig. 7 for different positions of the CCD camera. It can be seen that the predicted shape is almost insensitive to the position of camera when $x=3$ m and the camera moves in a direction parallel to the flame axis. When the camera is closer to the flame ($x=1$ m), the contours change slightly, and the flame length based upon the flame brightness appears to be smaller. Moreover, the axial displacement of the CCD camera influences the predicted contour and the axial location of the maximum brightness.

5. Conclusion

A mathematical model was described in this paper aimed at the prediction of the flame image/brighness in the visible spectrum range of a turbulent propane free jet flame. The model comprises a submodel for the calculation of temperature and absorption coefficient distributions and another one for the prediction of the flame image, using as input data the results of the first submodel. The first submodel is based on the numerical solution of the equations governing conservation of mass, momentum and energy. The second submodel is based on the integration of the radiative heat transfer equation along selected directions.

The model was applied to a propane flame for which experimental data were available. The predicted temperature profiles are in reasonable agreement with the measurements. The predicted flame brightness is in qualitative agreement with the digitized flame image and it is closely related with the absorption coefficient distribution. The position of the CCD camera influences the digitized flame when the camera is close to the flame; however, the influence becomes negligible at a distance of 3 m.

From the digitized flame image, several parameters related with the performance of the burning process (flame area, length, center of mass, maximum and minimum moments of inertia) may be computed. This information can be used for monitoring, classification and diagnosis. Therefore, the model may be regarded as a useful engineering predictive

tool with capability for on-line control of boilers and furnaces in the future.

References

(1) Victor, J., Costeira, J., Tomé, J. and Sentieiro, J., A Computer Vision System for Characterization and Classification of Physical Phenomena Inside Glass Furnaces, Proc. CIM-Europe Workshop CIM in the Process Industry, Athens, 20-21 June (1991).

(2) Launder, B.E. and Spalding, D.B., The Numerical Computation of Turbulent Flows, Comp. Meth. Appl. Mech. Eng., Vol. 3(1974), p. 269.

(3) Shabbir, A. and George, W.K., Energy Balance Measurements in an Axisymmetric Turbulent Buoyant Plume in a Neutral Environment, Sixth Symposium on Turbulent Shear Flows, Toulouse (1987).

(4) Pereira, J.C.F. and Rocha, J.M.P., Computation of Turbulent Jets and Plumes using Second Moment Closures, 7th Int. Conf. Num. Meth. Laminar and Turbulent Flow, Stanford(1991), p. 200.

(5) Elgobashi, S. and Launder, B.E., Turbulent Scales and the Dissipation Rate of Temperature Variance in the Thermal Mixing Layer, Phys. Fluids, Vol. 26, No. 9(1983), p. 2415.

(6) Nagano, Y. and Kim, C., A Two-Equation Model for Heat Transport in Wall Turbulent Shear Flows, J. Heat Transfer(1988), p. 583.

(7) Newman, G. R., Launder, B.E. and Lumley, J.L., Modelling the Behaviour of Homogeneous Scalar Turbulence, J. Fluid Mech., Vol. 11(1981), p. 217.

(8) Liew, S.K., Moss J.B. and Bray, K.N.C., Flamelet Modelling of Chemical Closures in Turbulent Propane Air Combustion, Report TP-84-81, School of Mech. Engng., Cranfield Institute of Technology(1984).

(9) Lockwood, F.C. and Naguib, A. S., The Prediction of the Fluctuations in the Properties of Free, Round—Jet, Turbulent Diffusion Flames, Combustion and Flame, Vol. 24(1975), p. 109.

(10) Abou-Ellail, M., Gosman, A.D., Lockwood, F.C. and Megahead, I.E.A., Description and Validation of a Three-Dimensional Procedure for Combustion Chamber Flows, Journal of Energy, Vol. 2, No. 2(1978), p. 71.

(11) Khan, I.M. and Greeves, G.A., A Method for Calculating the Formation and Combustion of Soot in Diesel Engines, Heat Transfer in Flames (Ed. Afgan and Beer) (1974), p. 391.

(12) Magnussen, B.F. and Hjertager, B.H., On Mathematical Modelling of Turbulent Combustion with Special Emphasis on Soot Formation and Combustion, 16th Symp. (Int.) on Combustion, The Combustion Institute, Pittsburgh(1976), p. 719.

(13) Lockwood, F. C. and Shah, N. G., A New Radiation Solution Method for Incorporation in General Combustion Prediction Procedures, 18th Symp. (Int.) on Combustion, The Combustion Institute (1981), p. 1405.

(14) Hottel, H.C. and Sarofim, A.F., Radiative Heat Transfer, (1967), McGraw-Hill, New York.

(15) Truelove, J.S., A Mixed Grey Gas Model for Flame Radiation, AERE Harwell, Report HL76/3448/KE(1976).

(16) Durão, D.F.G. and Pereira, J.C.F., Calculation of Isothermal Three-Dimensional Free Multi-Jet Flow, Applied Mathematical Modelling, Vol. 15 (1991), p. 338.

(17) Van der Hulst, H.C., Light Scattering by Small Particles, (1957), John Wiley & Sons, Inc., New York.

(18) Bohren, C.F. and Huffman, D.R., Absorption and Scattering of Light by Small Particles, (1983), John Wiley & Sons, Inc., New York.

(19) Felske, J.D., Hsu, P.F. and Ku, J.C., The Effect of Soot Particle Optical Inhomogeneity and Agglomeration on the Analysis of Light Scattering Measurements in Flames, J. Quant. Spectrosc. Radiat. Trans.(1986), p. 35.

(20) Viskanta, R. and Menguç, M.P., Radiation Heat Transfer in Combustion Systems, Prog. Energy Combust. Sci., Vol. 13(1987), p. 97.

(21) Siegel, R., Radiative Behaviour of a Gas Layer Seeded with Soot, NASA TN D-8278, Washington, D.C.(1976).

(22) Fernandes, E.C., Heitor, M.V., Simões, J.P. and Wei, J., On the Combustion Characteristics of Interacting Turbulent Jet Flames, Proc. 17th Eurotherm Seminar on Heat Transfer in Radiating and Combusting Systems, Cascais, Portugal, 8-10 October(1990).